# Time and Space Resolved Diagnostics for Plasma Thermal-Chemical Instability of Fuel Oxidation in Nanosecond Plasma Discharges

Aric C. Rousso<sup>1\*</sup>, Benjamin M. Goldberg<sup>2</sup>, Timothy Y. Chen<sup>3</sup>, Shuqun Wu<sup>3,4</sup>, Arthur Dogariu<sup>3</sup>, Richard B. Miles<sup>3,5</sup>, Egemen Kolemen<sup>3,6</sup>, Yiguang Ju<sup>3</sup>

<sup>1</sup>Department of Mechanical and Aerospace Engineering, Princeton University, Princeton, NJ 08544, USA Currently with Lawrence Livermore National Laboratory, Livermore, CA 94550, USA

<sup>2</sup>Department of Mechanical and Aerospace Engineering, Princeton University, Princeton, NJ 08544, USA Currently with the Combustion Research Facility, Sandia National Laboratories, Livermore, California 94551, USA

<sup>3</sup>Department of Mechanical and Aerospace Engineering, Princeton University, Princeton, NJ 08544, USA

<sup>4</sup>College of Automation Engineering, Nanjing University of Aeronautics and Astronautics, Nanjing, Jiangsu 210016, China

<sup>5</sup>Department of Aerospace Engineering, Texas A&M University, College Station, TX 77843, USA

<sup>6</sup>Princeton Plasma Physics Laboratory, Princeton, NJ 08544, USA

**Abstract** 

A thermal-chemical instability in a nanosecond pulsed dielectric barrier discharge (DBD) plasma

occurring in methane-oxygen-argon mixtures is experimentally observed and measured by 1-D time-resolved in-

situ electric field measurements. This instability, created by the positive feedback between plasma kinetics and

plasma-assisted low temperature fuel oxidation, is studied using electric field induced second harmonic

generation (E-FISH) and direct ICCD imaging. It is found that the chemical kinetics via plasma-assisted low

temperature methane oxidation causes a new type of plasma instability, a thermal-chemical instability, by rapid

formation of streamers from an originally uniform discharge. The results also revealed that the occurrence of a

thermal-chemical instability in a reactive flow drastically changes the plasma properties by forming multiple

secondary discharges and leads to micron sized non-uniform electric distributions. The electric field of the micron

sized streamers is much greater than the average electric field. Furthermore, one-dimensional data analysis shows

the positive feedback loop between the streamers and the low temperature plasma assisted oxidation chemistry in

the plasma thermal-chemical instability. The present finding advances the understanding plasma instability

growth and provides a new way to control plasma uniformity in plasma-assisted combustion and plasma fuel

reforming.

Keywords: Electric field measurements, second harmonic generation, plasma assisted oxidation,

nanosecond pulsed DBD plasma discharge

2

### 1. Introduction

As the world transitions to low carbon energy, the increasing intermittency of renewable energy provides a great opportunity to convert fossil energy into low carbon chemicals [1] and materials [2–4] using non-equilibrium plasmas. In addition, to develop advanced lean burn engines with low carbon emissions, it is critical to control plasma properties to achieve efficient ignition [1–5]. For these applications, diffuse, volumetric, nonthermal discharges are needed to meet high chemical reactivity, low power consumption, and high efficiency [5–7]. Therefore, it is of great importance to understand the mechanism of plasma instabilities in a chemically reactive flow.

Several mechanisms of plasma instabilities such as the secondary-electron-emission instability [8], universal instability with a magnetic field in an inhomogeneous plasma [9], and plasma thermal instability via Joule heating [10] have been reported. For a plasma thermal instability, as shown in Figure 1, the positive feedback between the change in electron number density ( $n_e$ ), Joule heating (jE, a product of current j and electric field E), temperature (T), gas number density (N), and the reduced electric field is expressed as,  $n_e \uparrow \rightarrow jE \uparrow \rightarrow T \uparrow \rightarrow N \downarrow \rightarrow E/N \uparrow \rightarrow n_e \uparrow$ . The plasma thermal instability mechanism has been studied in noble gases and air [10–13]. However, the mechanism of plasma instabilities during discharges that occur in chemically reactive and combustible mixtures is not well-understood. As shown in Fig. 1, in a chemically reactive flow, the elementary chemical reactions in the process such as the electron impact fuel dissociation, electron attachment affected by oxygen

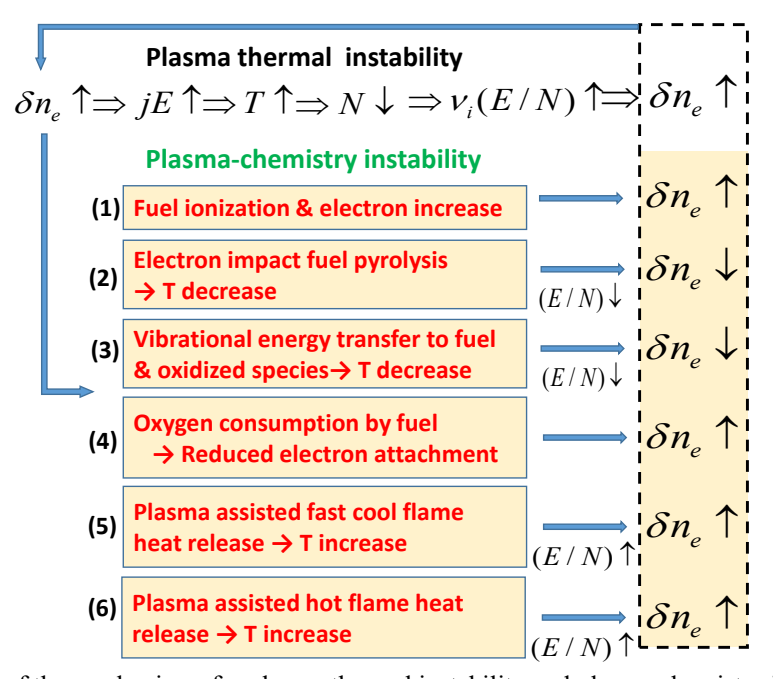


Figure 1: Schematic of the mechanisms for plasma thermal instability and plasma chemistry instability.

consumption and water formation, species changes in the plasma-assisted reaction process, and plasma-assisted low and high temperature fuel oxidation [14, 15] also contribute to either negative or positive feedback of the change of electron number density. In fact, in an early experiment of energy coupling to the plasma of repetitive nanosecond pulse discharges in a reactive ethylene/air mixture [16], it was clearly shown that the plasma instability of a reactive mixture developed much faster than that in air. The mechanism for plasma instability in this reactive mixture, however, was not investigated.

To understand plasma instability in a reactive flow, several studies have explored methods to eliminate the instability [12, 17–19] through the use of different bath gases. The results showed that there is a profound effect on the uniformity of the plasma due to changes in thermal and mass diffusivity. It has also been shown that the plasma instability can be mitigated by either preheating the gas or raising the mixture temperature [16–18]. While these experimental studies provide useful observations of plasma instability, the cause of this instability formation in a chemically reactive flow remains unclear. Recently, with a hypothesis of plasma chemistry instability, the authors numerically studied the contraction process in a fuel-lean H2/O2/N2 mixture with a simple plasma combustion kinetic model [20]. The results showed clearly that there is a plasma thermal-chemical instability and the elementary reactions of combustion kinetics can either decelerate or accelerate the occurrence of plasma instability. However, to date, few detailed experimental diagnostics have been carried to understand the physical process of plasma chemical instability formation.

Significant progress has been made in the development of new techniques to quantify the dynamics and properties of non-equilibrium plasmas. For example, the electric field measurements using electric field induced second harmonic generation (E-FISH) with a ultrashort pulsed laser has made it possible to measure time-dependent electric fields in a non-equilibrium plasma [6, 21, 22]. Briefly, second harmonic generation is impossible in a centrosymmetric medium. However, in the presence of an electric field, the inversion symmetry is destroyed allowing for a coherent buildup of radiation at the second harmonic frequency of an intense laser source. The effect was first discovered in the 1960's and 70's and has mostly been used to measure the hyper polarizability of different molecules [23, 24]. The method was first used to measure an arbitrarily applied electric field in 2017 [22]. Since then, several groups around the world have adopted the method using femto-, pico-, and nanosecond laser pulses for measurements in a variety of plasma discharges [21, 25–28]. To date, the majority of transient electric field measurements have been limited to zero dimensional cases, representing a limitation on the use of the method for highly transient plasmas. Therefore, there is a clear need to develop a time and space resolved diagnostic method to understand the dynamics and properties of plasma chemistry instability [29, 30].

The goal of this paper is to explore this plasma thermal-chemical instability and probe key plasma properties to understand time evolution of its growth. This study will utilize recent *in-situ* E-FISH measurement techniques to measure the spatially resolved electric field along with ICCD images and Rayleigh scattering for plasma uniformity and temperature measurements. Using argon as a bath gas, with either methane, oxygen, or a methane/oxygen mixture added, the effect of these gas additions on the electric field and temperature profiles are measured. Broadband ICCD imaging is also recorded to explore the feedback effect of plasma filamentary constriction due to hydrocarbon oxidation. The results will show the distinct constriction and formation of non-uniform behavior solely due to the addition of hydrocarbon chemistry, as well as exploration into the parameter space and possible reasons for this phenomenon.

## 2. Experimental methods

The experimental apparatus, Figure 2, has been reported previously for related experiments [31–33]. A rectangular quartz cell has been constructed with a plane-to-plane dielectric barrier discharge area of 44.5 x 44.5 mm square. The quartz has a dielectric constant of 3.78 and a thickness of 1.6 mm covering each metal electrode, with a quartz to quartz gap distance of 14 mm. Removable windows at the ends of the cell allows for coupling of various laser and imaging diagnostics in the direction of flow, while the quartz walls in the discharge region also allow for measurements in the direction perpendicular to the flow. All experiments maintained initial room temperature and a pressure of 50 Torr within the reactor. Total flow rates are 0.7 m/s for all conditions, with a plasma residence time of ~0.06 seconds. The fuel and oxygen mole fractions are held constant for all cases

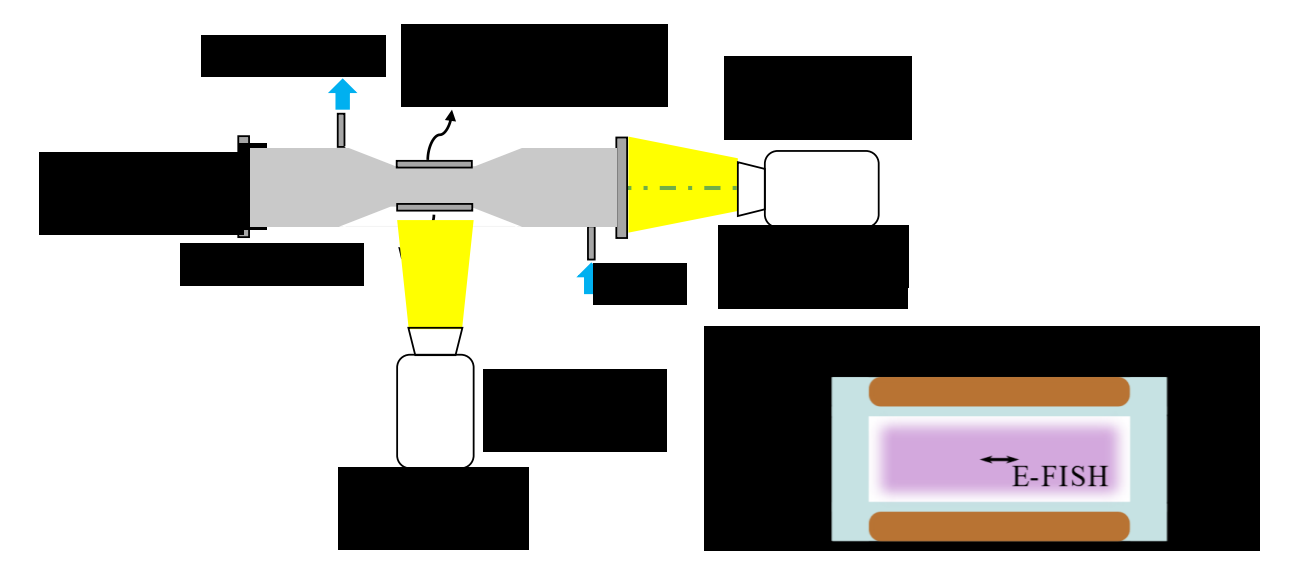


Figure 2: Experimental Setup. Laser based diagnostics are setup in the direction of flow. Cameras are positioned either looking down the flow field (streamwise), or perpendicular to the flow (orthogonal). A schematic of the discharge with relevant dimensions is shown in the streamwise direction, along with the spatial position of the E-FISH diagnostic.

discussed below, with argon added to fill the remaining mole fraction if one of the mixture components is removed. Three cases are studied: a stoichiometric fuel/O<sub>2</sub> case (6.6% CH<sub>4</sub>, 13.4% O<sub>2</sub>, 80% Ar), a pyrolysis case (6.6% CH<sub>4</sub>, 93.4% Ar) and a no fuel case (13.4% O<sub>2</sub>, 86.6% Ar). A nanosecond-pulsed power supply (FID GmbH FPG 30-50MC4) is used for plasma generation, with a maximum repetition frequency of 30kHz, FWHM of 12 ns, and maximum peak voltage of 32 kV, which is operated in a burst mode via an external digital pulse generator (SRS DG645). A burst of 150 pulses at 30 kHz pulse repetition rate is used, with a total discharge time of 0.005 seconds for a single burst of pulses. The bursts are operated at 15 Hz, which allows for gas replenishment and to prevent coupling between bursts while minimizing data collection times.

Several diagnostics have been utilized in the present work. For imaging subsequent pulses within a single burst, simultaneous images of the plasma are taken using two PCO Dimax HD sCMOS cameras both in the streamwise as well as orthogonally to the direction of flow (see Fig. 2). Single shot images monitoring every pulse within a single burst are taken at 30 kHz with a gate of 1 µs for analysis of filament formation and growth within the given burst. For nanosecond resolution of the growth of a single pulse within the plasma burst, a CCD camera coupled to a LaVision PicoStar intensifier was used, with a gate of 1 ns, which provides time-dependent resolution into the pulse formation. Note that these images are not correlated for a single burst event. Thus, a total of 5 images were taken for each time point, for average comparison as well. These nanosecond images are only taken in the streamwise direction. Simultaneous voltage measurements are made using a Tektronix P6015A high voltage probe.

Electric field measurements are performed using the electric field induced second harmonic generation method (E-FISH) [21, 22, 29, 34, 35]. The E-FISH setup in this experiment was similar to that used in our previous work [21, 22]. Briefly, a Spectra-Physics Solstice Ace femtosecond laser is used with a peak energy of ~7 mJ per pulse, centered at 800 nm and bandwidth of 15 nm, pulse duration of 60 fs, and a nominal beam diameter of 10 mm is used as the pump laser source. The beam is focused into the discharge region using an f = 400 mm cylindrical lens in the direction of gas flow. This creates a measurement volume of ~25 µm x 1 cm x 2 cm (beam waist x beam diameter x confocal beam parameter). The second harmonic light is collimated using a matched cylindrical lens, and the pump and second harmonic light are then spectrally separated using a dispersion prism. The second harmonic signal beam is focused directly onto the photocathode of a PIMax4 1024i ICCD using a third, cylindrical lens allowing for 1-D electric field imaging. Images are collected in a single shot fashion, and time-binning and averaging is completed in a post processing routine. Calibrations are taken on a per-pixel basis, with the minimum detectivity around 1 kV/cm.

Rayleigh scattering was performed in a setup previously used for Thomson scattering [33]. A Quantel Q-smart 850 Nd:YAG laser with pulse width of 6 ns and pulse energy of 380 mJ was focused into the center of the rectangular quartz cell described above. For centerline measurements, apertures were put in place to reduce the amount of stray light. Plasma emission was filtered by a 532 nm bandpass filter with full width at half maximum of  $\pm$  1 nm. The filtered light is then imaged onto a PIMAX 1300 ICCD with a 20 ns gate width. Through direct imaging, a 1-D measurement along the laser propagation direction was captured with ~100 $\mu$ m resolution per pixel.

For the Rayleigh scattering, E-FISH and nanosecond resolved ICCD imaging, pulses 1-5, 10, 25, 50, 75, 100 and 110-150 were analyzed for the oxidative  $CH_4/O_2/Ar$  case. Pulses 1, 2, 10, 50, 100, and 150 were measured for the  $CH_4/Ar$ , and  $O_2/Ar$  cases, as the plasma was uniform and showed no evidence of filament formation.

### 3. Results and Discussion

# 3.1. High speed imaging of the 150 pulse plasma burst

CMOS images (10 µs gate) of pulses 10, 50, 75, 100, 125 and 150 within a single burst of pulses along the axis of flow (streamwise) for each mixture are shown in Figure 3. The 3 cases of plasma discharge in three different mixtures are compared to show qualitatively the effect of mixture composition and plasma assisted chemical reactions on plasma instability. Both the pyrolysis (6.6% CH<sub>4</sub>, 93.4% Ar) and no fuel (13.4% O<sub>2</sub>, 86.6% Ar) cases clearly have uniform discharges throughout the burst. There is a known difference in intensity here due to the change in the argon mole fraction, as well as the weakening of the discharge due to electron attachment reactions caused by the addition of oxygen to the plasma [10]. For the oxidative case (6.6% CH<sub>4</sub>, 13.4% O<sub>2</sub>, 80% Ar), however, where low temperature methane oxidation are initiated through plasma-assisted reaction pathways, [1] filamentation is observed. This filamentation (instability) does not occur immediately, as there is still a diffuse discharge in early pulse numbers within the burst, but with increasing pulse numbers, the discharge grows increasingly filamentary. The transition to distinct filaments seems to occur somewhere between pulse 75 and 100. As seen in the videos presented in the supplementary materials, these bright filaments are clearly due to constriction of the diffuse discharge into these filamentary channels, as the surrounding area grows gradually dimmer while the filament strengthens from pulse to pulse. Note that, as stated above, the intensity scaling for a given set of images is kept constant, so this is dimming of the region between filaments, not an adjustment in scale. The filaments are consistent in a single burst from pulse to pulse: once formed in a particular location, they are stable until the burst ends and the gas is refreshed. The filaments on the sides of the electrodes do tend to be

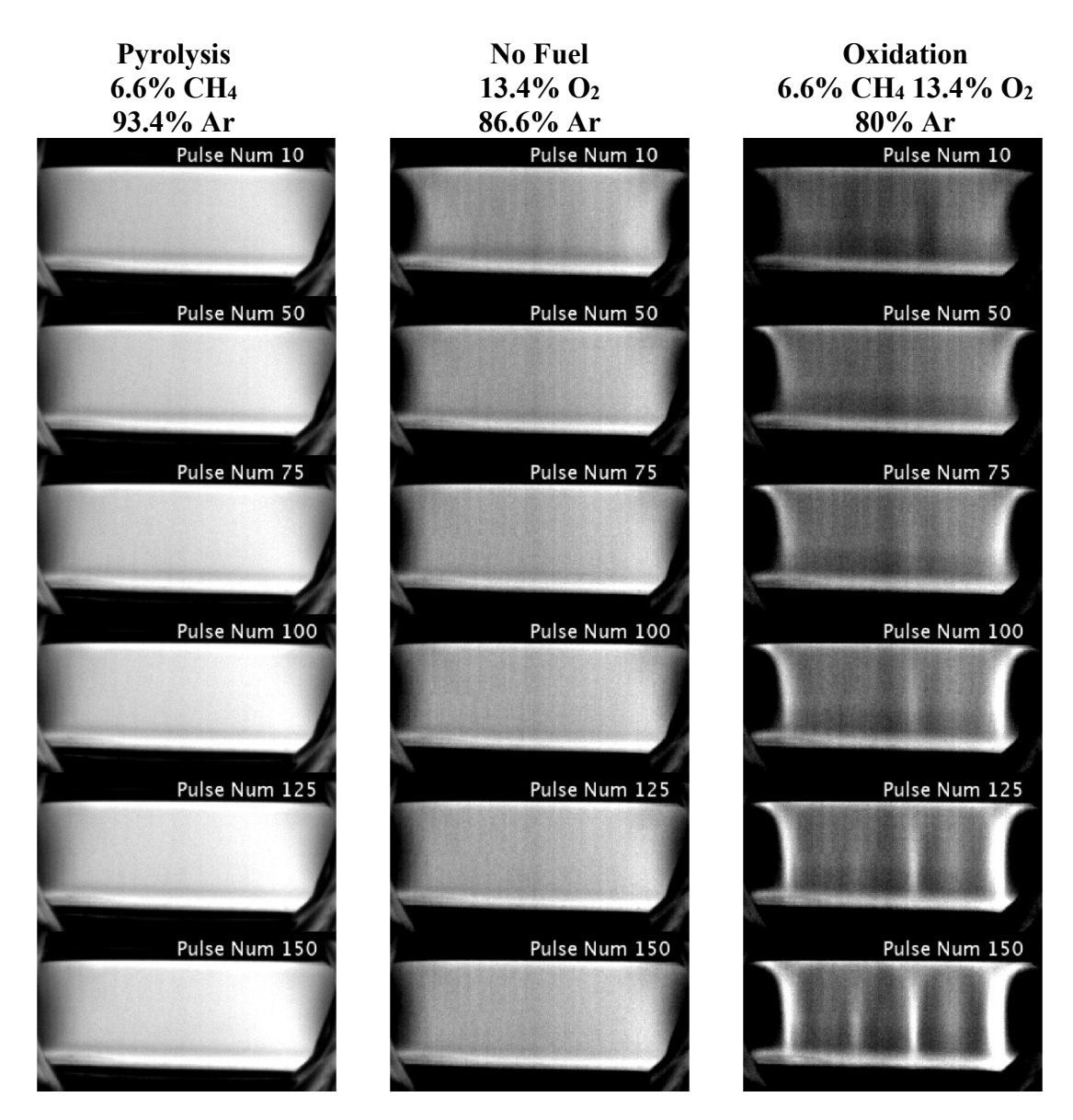


Figure 3: CMOS images of a single burst of the plasma discharge. The fuel and oxygen mole fractions are held constant (6.66% CH<sub>4</sub>, 13.34% O<sub>2</sub>) with argon added to fill the remaining mole fraction when a mixture component is removed. Intensities are not to scale, with the pyrolysis case and no fuel brightness reduced to prevent saturation.

stronger, more stable and more repeatable, likely caused by plasma edge effects. For the remainder of the discussion this work, these edge formations will be ignored to focus on the center plasma filaments, as they are formed solely due to the plasma-combustion interaction as opposed to additional geometric factors. Therefore, the present experiment clearly confirmed the existence of plasma thermal-chemical instability proposed in our previous study[2].

Figure 4 shows pulse 150 for the oxidative case, taken with the same camera conditions for four different bursts. It can be seen that aside from the edge effects, the filaments move in location from burst to burst, as predicted in the literature [10]. The strongest filament does seem to appear on the right side of the image more

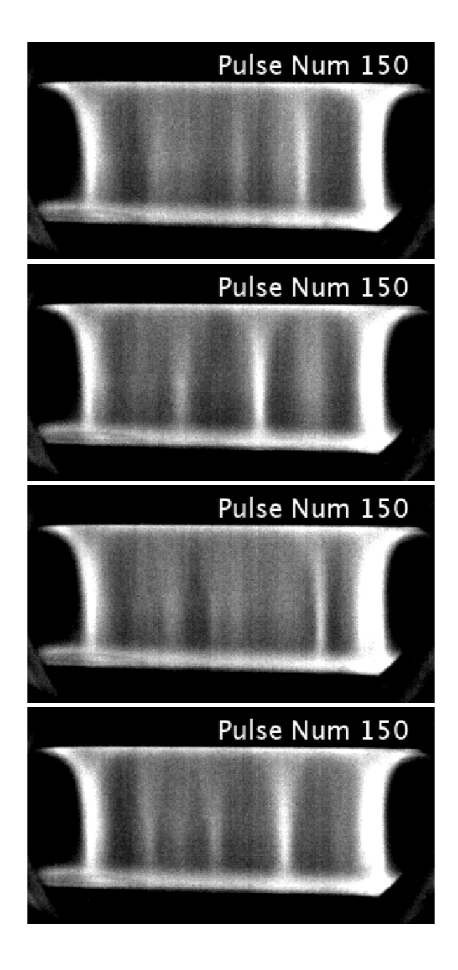


Figure 4: Snapshots of pulse 150 from various bursts in the streamwise direction. Filament location is seen to be moving from burst to burst.

often, which may be due to slight deformities in the cell construction such as non-uniformities in the quartz or electrode gap distance. The random movement of the filament does confirm, however that these constrictions are due to a chemical coupling caused by the oxidation reactions, and not due to the geometry or irregularities of the cell itself, which are weak enough in this case to just preferentially determine a larger region where the strongest filament might form.

# 3.2. Imaging of longer pulse count bursts at 1 Hz

Image sequences were also taken at 1 Hz instead of 15 Hz burst frequency to allow for more pulses in the burst. The plasma was still operated at 30kHz pulse frequency, but with up to 3000 pulses per burst. The filaments in these cases take longer to form, and non-uniformity is not seen until approximately pulse 200. The flow rates in all cases is fast enough to allow for replenishment of the mixture in the discharge region between bursts, so this difference is due to charge effects, where the longer wait between bursts in the 1 Hz case gives time for some form of ion/charge recombination, as opposed to a thermal effect, as increasing bulk temperature has been shown

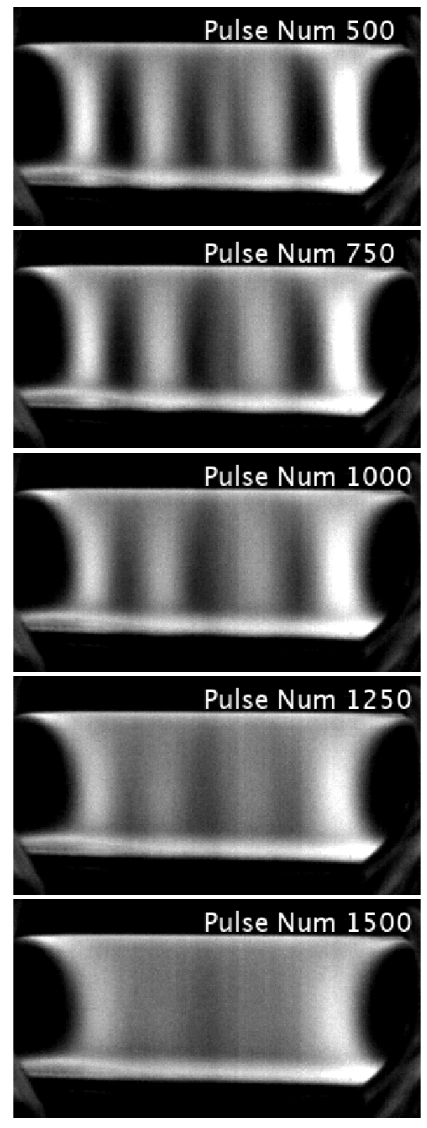


Figure 5: 10 µs CMOS images of various pulses within a longer 3000 pulse burst in the streamwise direction operated at 1 Hz. The plasma filaments are seen to form then smooth out

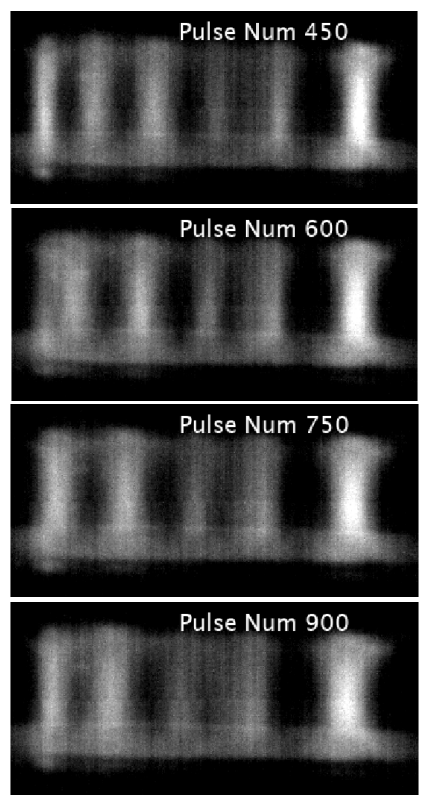


Figure 6: 10 µs CMOS images of various pulses within a longer 3000 pulse burst in the orthogonal direction operated at 1 Hz. Filaments are seen to move with the bulk flow, albeit at a slower velocity.

to increase the stability of the plasma not causing additional filamentation [18]. Additionally, the inter-burst time at 15 Hz is ~0.062s, compared to the 0.005s burst, which is significantly longer than the time required for the temperature to return to ambient as seen from previous studies [31, 36], so even at 15 Hz each burst has the same initial temperature and pressure conditions. Previous work has demonstrated that surface charges can last for tens of seconds or longer in a plate-to-plate DBD [37, 38], so this difference should not be due to surface charge effects either. At longer pulse counts, as seen in Figure 5, the thinner filaments coalesce into larger filaments, with the distinction between individual filaments growing significant more pronounced and darker regions without emission forming between the filaments. As the discharge continues, however, the filaments begin to blur and remerge, until by pulse 1500, there is a quasi-uniform discharge again. This demonstrates that this instability likely

has some thermal coupling, as thermal diffusion will result in a more uniform temperature profile at longer pulse counts, which reduces the magnitude of the local heating compared to the background temperature.

If we look in the orthogonal direction to the flow, as seen in Figure 6, filamentary modes are also seen, suggesting that these are narrow channels and not "striations" along the direction of flow. From this viewpoint, the pulses move in the direction of the flow, although slower than the bulk velocity of the flow; anywhere from 0.5-0.8x the average flow speed. There appears to be some effect of mass diffusion, as the filaments seem to bulge/bow downstream at later times. Again, strong filaments are seen at the edges of the discharge, and these do not move with the flow, although filaments are seen to merge with and separate from the edge filaments. These plasma channels also re-broaden with later pulses, until a mostly uniform discharge is seen, similar to the streamwise images. These longer data sets, therefore, show that the plasma instability is thermally coupled, and possibly chemically coupled as well, as the filaments move in the flow field with the mixture, but not at the speed of the bulk gas.

## 3.3. Nanosecond resolved images of pulses within the 150 pulse burst

A 1 ns gate ICCD camera was used to image the formation and duration of these structures in a single pulse within the burst compared to the diffuse plasma. Ten images were taken at each time point, with a 1 ns step starting from 10 ns before the trigger pulse, out to 140 ns. Images in this case are still correlated in brightness, but each image is from its own individual burst. As stated above, voltage measurements were concurrently recorded for each pulse, along with the trigger for the camera, and is shown below the image, as can be seen in Figure 7. Time t = 0 is set to 10% of the maximum voltage for waveform comparison, and to account for slight jitter in the interpulse timing, on the order of  $\sim \pm 5$  ns. A delay of 8 ns was added to the imaging data, accounting for internal processing and cable lengths, to correlate the initial emission from the plasma with the breakdown seen in the voltage waveform. The 1 ns time step between images, however, is well known, due to the low jitter (< 25 ps) of

the pulse generator (SRS DG645). For this data set, all time points will be referenced from the determined zero point, as  $\Delta t$  values.

Figure 7 shows pulse 75 and pulse 100 for the oxidation case at the same time instant of  $\Delta t = 12$  ns. As is shown both in Fig 6 and by the videos in the supplementary material, the plasma is uniform for early pulses and transitions to distinct filaments somewhere between pulse 75 and 100, as discussed previously. Further evidence is shown here, where with nanosecond resolution distinct filamentary structures are seen in pulse 100. Pulse 75 is starting to show some non-uniformities in overall structure, especially compared to the no fuel and pyrolysis cases, but the diffuse plasma nature is still present, especially when compared to later observed filamentary pulses.

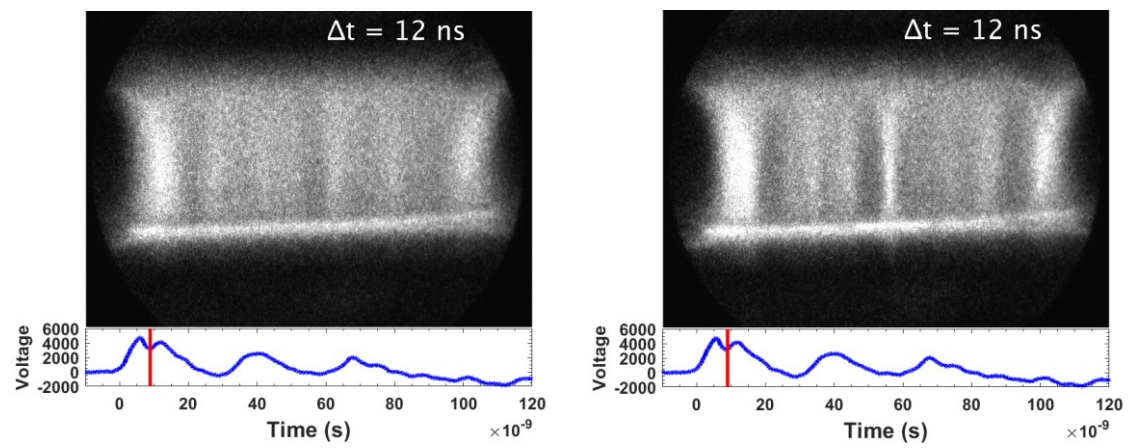


Figure 7: Nanosecond-resolved ICCD image of pulse 75 (right) vs pulse 100 (left) in the CH<sub>4</sub>/O<sub>2</sub>/Ar oxidative discharge case. Slight variation in intensity is seen at pulse 75, but significant filamentation is seen by pulse 100.

Figure 8 shows several time instances of pulse 150 for the methane oxidation case, again with ns time-resolution. By this point the plasma is completely nonuniform, with initial emission seen when  $\Delta t$  is 9 ns. Compared to the previous data for pulse 100 in Fig. 7 at  $\Delta t = 12$  ns where most of the plasma is uniform, even the initial emission is seen to be filamentary in nature. By  $\Delta t = 12$  ns in this case, the plasma is fully established, with the individual filaments connecting at the walls. As the voltage drops, the emission begins to decrease through  $\Delta t = 16$  ns, with only faint emission seen at the strongest channels for  $\Delta t = 20$  ns. By 26 ns, only faint emission is seen at the walls, likely due to residual surface charge, and afterglow in several of the channels. These images reveal that the filaments dominate the discharge structure at this point, with the blurring effect seen in the earlier

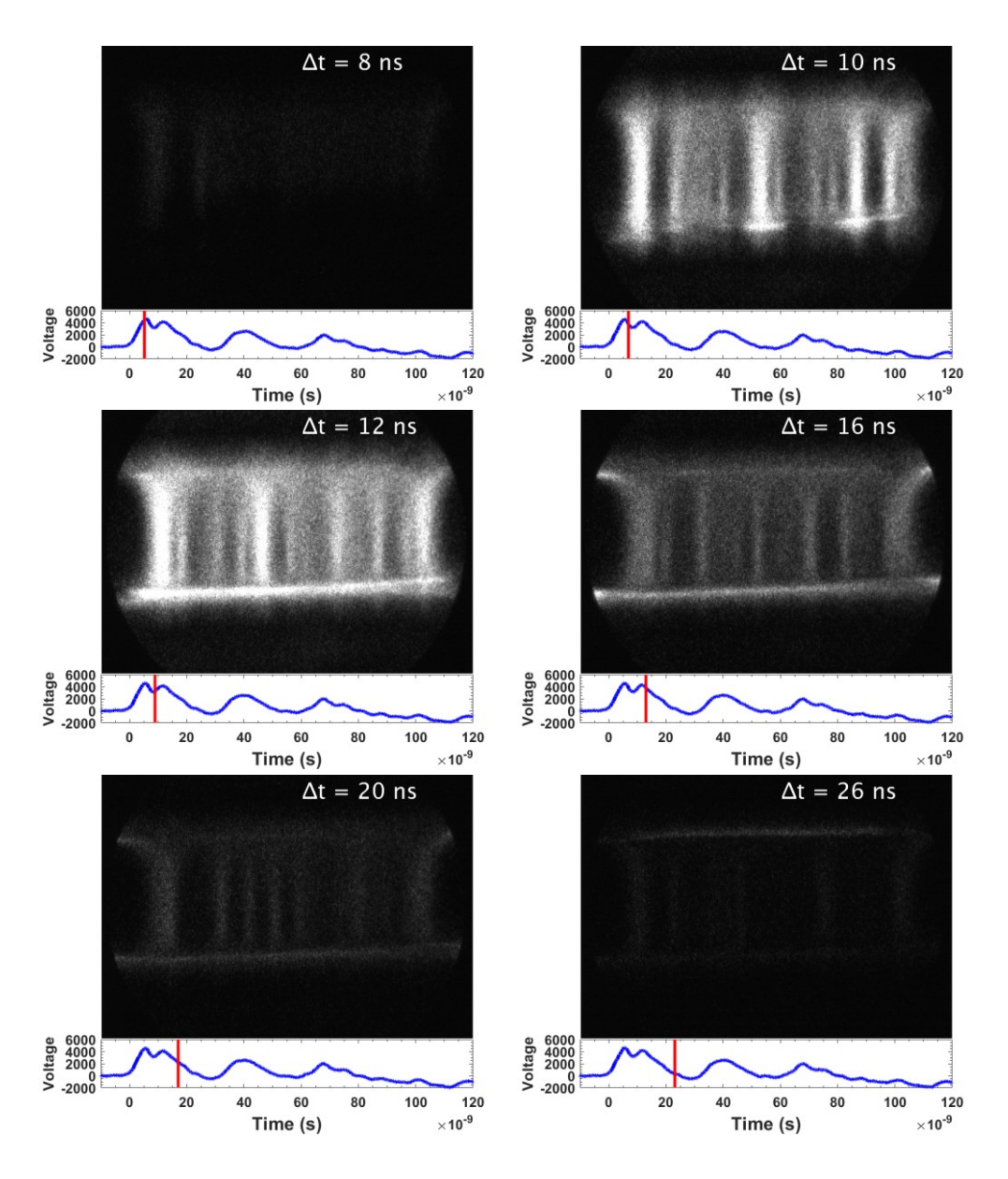


Figure 8: Nanosecond-resolved ICCD image of pulse 150 at various time steps in the  $CH_4/O_2/Ar$  oxidative discharge case. The discharge in this case starts filamentary, and lasts around 12 ns, with some emission at the

10 μs images due to the longer imaging time. Between pulse 100 and 150, then, we see a regime change from beginnings of filaments to full constriction and an entirely non-uniform discharge structure. Overall emission seems to follow well with the voltage waveform, with an approximate duration of ~10-15 ns. This is slightly longer in the pyrolysis case, as the additional argon mole fraction seems to extend the relaxation time compared to the no fuel and oxidative cases. The secondary voltage pulses seen in the waveform data do not seem to result in significant emission, suggesting that these secondary pulses, still with significant voltage applied, do not result in volumetric breakdown and subsequent emission. As will be discussed later, however, these voltage pulses still show some electric field present in the plasma, so may be sub-breakdown energy deposition at lower E/N values and could still play a role in the chemical kinetics through vibrational pumping.

# 3.4. Measurements of changes in local electric field using E-FISH

The time-dependent electric field during the nanosecond pulses was measured using the E-FISH method. The electric field measurements for pulses 10, 100, and 150 are shown as the red points in Figure 9 for the 3 discharge cases, while the concurrently measured high voltage waveforms are shown as the blue lines. This data is the spatially averaged electric field across the 1-D measurement region as well as the average of all the shots taken at each time point. For the Ar/CH<sub>4</sub> discharge, the strongest of the 3 discharges and which the plasma imaging confirmed to be diffuse, there is good agreement with the initial high voltage rise, followed by a sharp reduction in the electric field slightly offset from the applied voltage. This is consistent with a breakdown event, where the drop is due to the gas mixture ionizing and becoming conductive. The additional pulses seen after the main pulse in the high voltage waveform have been confirmed to be voltage applied across due to the pulser supplying secondary pulses. In this mixture, very little secondary electric field rise is shown, due to the volumetric breakdown, and the charge accumulation in the sheath shielding the bulk plasma from the field changes. The third and final pulse does exhibit a small increase in the field, likely due to a reduction in the electron number density. Imaging does reveal faint discharge during some bursts corresponding with this second rise, indicating secondary breakdown can occur with strong enough field.

The middle plot shown in Fig. 9 is the electric field development for the Ar/O<sub>2</sub> case. While the results are similar to the Ar/CH<sub>4</sub> data, the smaller secondary pulses seen in the high voltage waveform have a larger accompanying field, likely due to lower electron density than the pyrolysis case. Due to attachment, the O<sub>2</sub> addition scavenges electrons quickly, reducing the plasma density. At the later times, there are not enough electrons to fully shield the secondary pulses, allowing for the stronger electric field present. Finally, the right plots shown in Fig. 9 demonstrate the oxidation case. Here, it can be seen that the initial pulses have much weaker shielding, and the field in earlier pulses follows the voltage waveform. While damping still does occur, these secondary pulses are very active even through pulse 150. Clearly, oxidation chemistry is scavenging electrons and changing the plasma process. It is important to note that with secondary field, there is also additional energy deposition in the bulk plasma, as lower E/N values will pump vibrational modes, which could possibly extend or enhance oxidation kinetics.

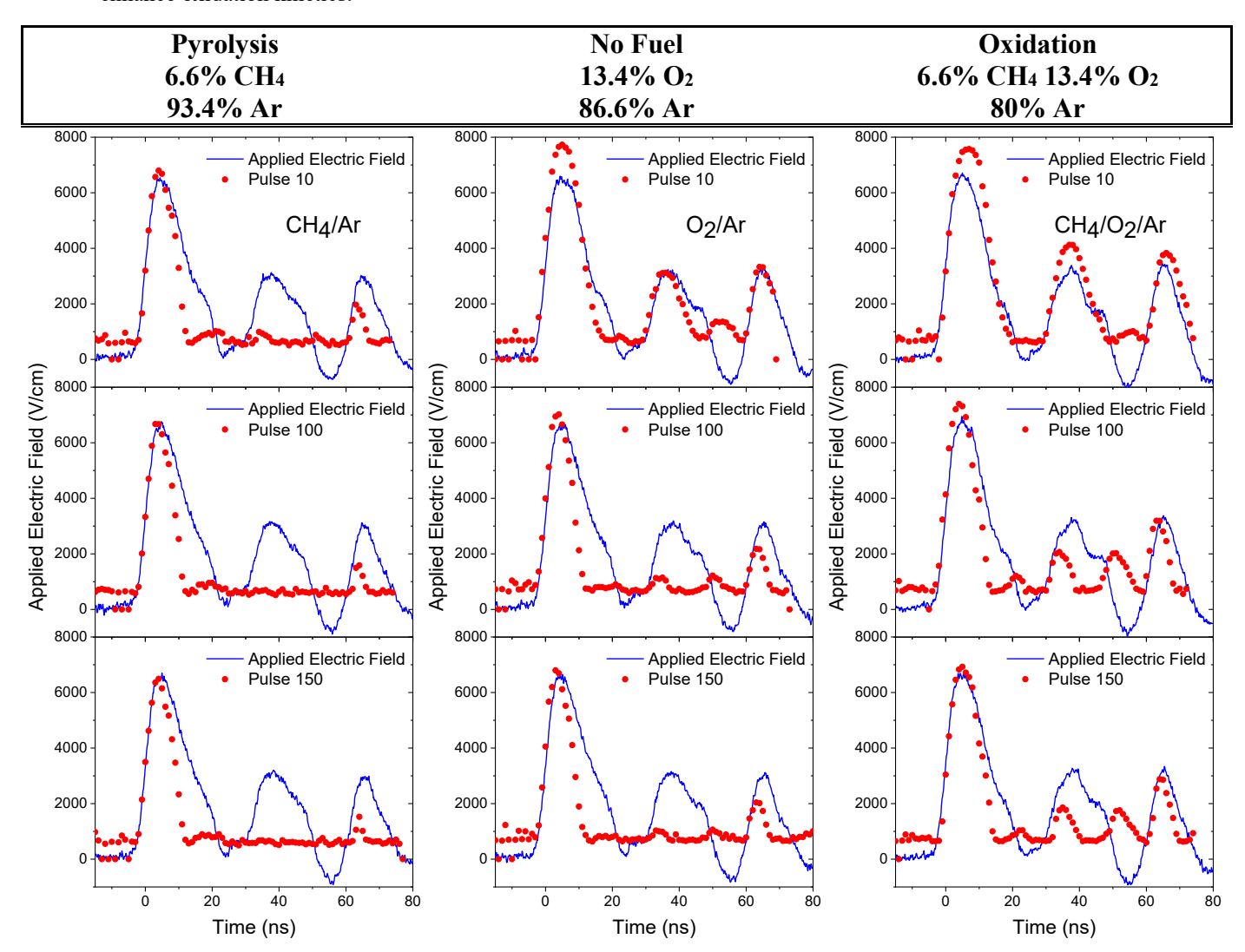


Figure 9: E-FISH data from pulses 10, 100 and 150 for the pyrolysis, no fuel, and oxidation cases of the plasma discharge. The pyrolysis plasma is the strongest, with the most argon, and dampens out the field effects of the later pulses due to a strong sheath. Oxygen acts as an electron scavenger, which allows for field effects to be felt in the bulk plasma in the other two cases.

The results presented above demonstrated the time and space averaged electric field measured across the femtosecond laser sheet. In order to further elucidate the effect of oxidation chemistry, we attempt to resolve the electric field with 1-D spatial accuracy across the ~5 mm width in the center of the plasma, as seen in Fig. 2. Unfortunately, shot-to-shot uncertainty in the E-FISH method does not allow for absolute single shot measurements as the calibration requires significant build-up of shots. For this reason, the relative single shot E-FISH profile at t = 3 ns on pulse 140 is shown in Figure 10. The profile has been normalized to the average signal count across the laser sheet. Some evidence for increased electric fields may be seen in the raw signal count data. In Figure 9, the different colors represent single shot measured values, with the mean given by the thicker black line. The individual spikes appear to be regions with significantly higher local electric fields as the E-FISH signal follows the square of the local field. Even still, there are several caveats to this. First, these spikes are also seen in the methane and oxygen datasets, albeit at much lower intensities and frequency of occurrence. It is possible these are real signals, in which case there is also fluctuation in the electric field in the other two cases, which would need to be explored further. Second, the electric field measurement is inherently spatially averaging along the laser path, as it generates signal along the entirety of the beam confocal parameter, which for this focusing is ~2 cm. For the current experiment, this entire range is within the plasma discharge region by design, but this

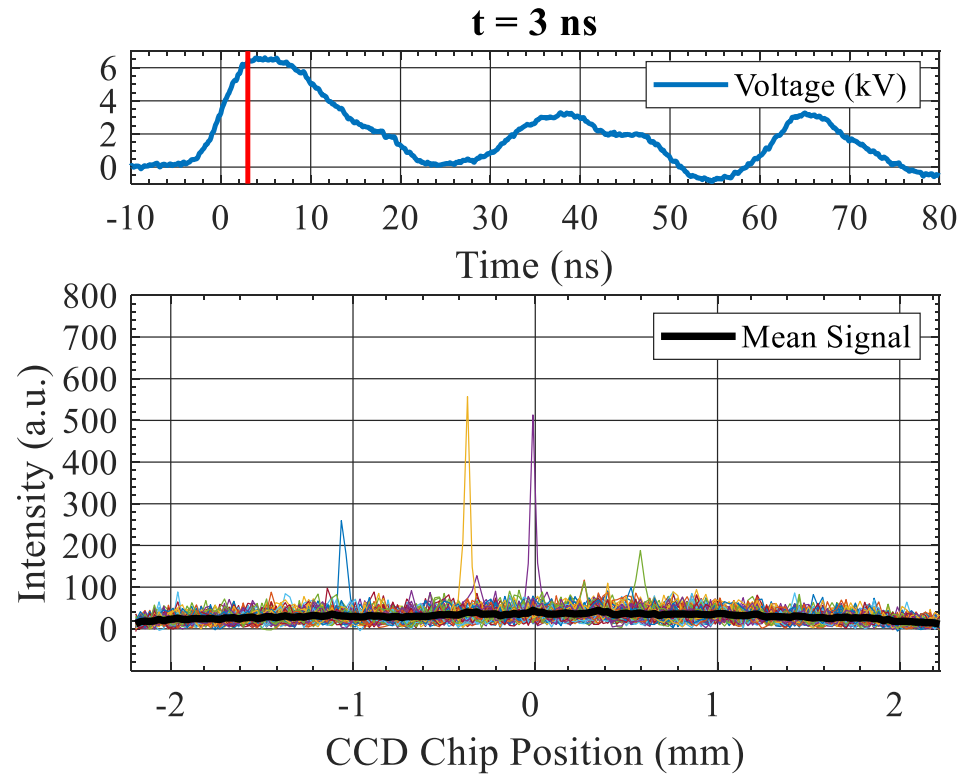


Figure 10: Multiple 1-D single shot E-FISH intensity counts and corresponding location in the voltage time-dependent waveform for pulse 140, 3 nanoseconds after the start of electric field rise. Mean signal is shown by the thick black line.

makes it difficult to study the apparent spikes that may be present due to these filaments. While it is clear for the plasma as a whole that chemistry is changing the plasma parameters, further study is certainly required with a spatially stationary filament to determine whether these filaments are physical. If so, then there are local chemical regions experiencing a much stronger electric field that that of the average measured in this study, which clearly could explain the filamentary behaviour observed. To what extent the combustion oxidation is in turn affecting the localized electric field through a feedback loop, however, is still an open question.

## 3.5. Rayleigh Scattering measurements to determine number density

Finally, measurements of the bulk gas number density were taken to try and look at the heating going on in the plasma. Previous studies [31–33] in the lab have demonstrated that oxidation chemistry clearly contributes to the bulk gas heating during the plasma burst, with up to 50% higher temperature rise in the oxidation case compared to an oxygen or pyrolysis plasma. Figure 11 shows the number density in the plasma as a function of pulse number for the CH<sub>4</sub>/O<sub>2</sub>/Ar oxidation case. Assuming the ideal gas assumption is maintained, this results in the temperature rise seen by the right-axis temperature scale. The error bars were calculated using a 5% uncertainty in the laser pulse energy which directly translates to uncertainty in the measured Rayleigh image intensity. Even with the error bars due to the uncertainty of the measurement, there is a clear temperature rise, very consistent with previous data, throughout the burst [32, 33]. This bulk temperature rise is too low to fully dampen the instability formation. As previous data has shown the temperature rise for argon plasmas similar to this to be

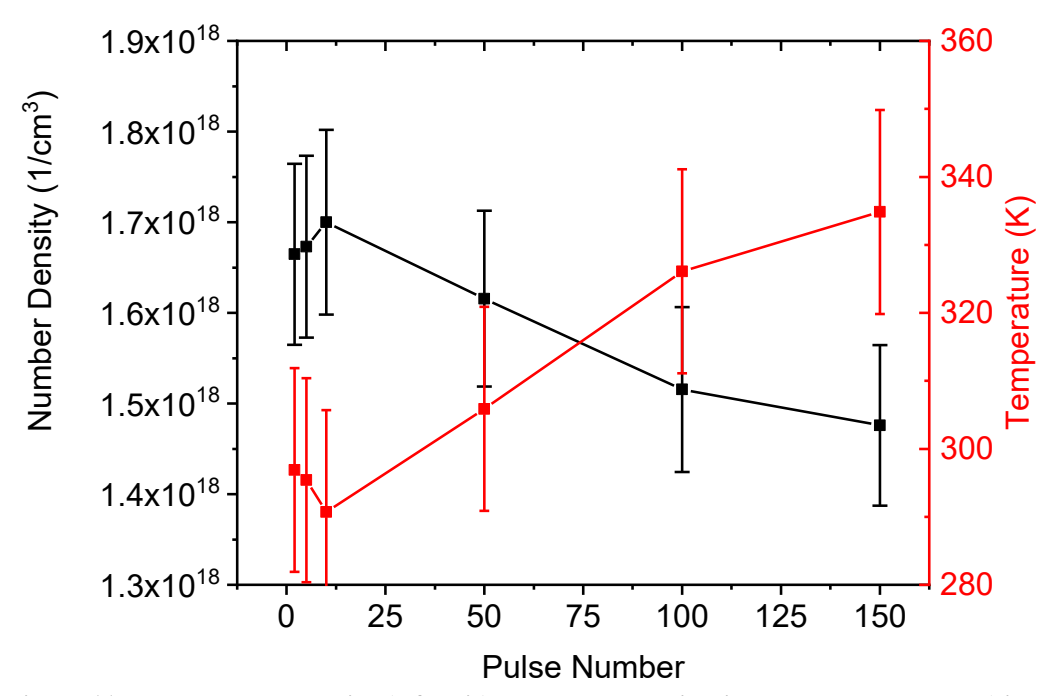


Figure 11: Bulk number density (left axis) and corresponding ideal-gas temperature (right axis) as a function of pulse number for the 150 pulse burst in the  $CH_4/O_2/Ar$  case. Data has been averaged over 100 shots. The error was determined by using 5% as the uncertainty in the laser pulse energy.

roughly linear, extrapolation out to 1500 pulses reinforces the earlier discussion that bulk heating helped remove the instabilities at longer pulse numbers [31, 36]. The much higher temperature from longer bursts provides an increase in mass diffusion, and also makes the local disturbance a smaller fraction of the overall temperature, resulting in a more uniform plasma.

Rayleigh scattering is also capable of 1-D spatially resolved measurements, but along the flow direction of the discharge region, opposite the direction of the E-FISH measurement. As seen from the images, however, these filaments are appearing in both spatial directions, so similar to the E-FISH, fluctuations of temperature should be visible. No large fluctuations of number density were seen for the present conditions, however. To ensure laser overlap with the filaments, a series of measurements were taken, both spatially at 1 mm steps across a 1 cm range as well as temporally, at 1 ns increments, for pulse 150 of the oxidation case, where the filaments were seen to be the most severe. When averaged, all of this data falls within the error bars for pulse 150 in Fig. 11. A subset of the raw data, presented as a fraction of the signal I to the background data I<sub>o</sub> can be seen in Figure 12, with the average measurement in black. While there is significant noise in this data, no large spikes are seen for any given run, like was observed in the electric field data. This has two possible sources of uncertainty that could explain this, similar to the discussion in the last section. First, the experiment may lack enough spatial resolution to accurately capture the filaments. It has been demonstrated in the literature that these channels can be extremely

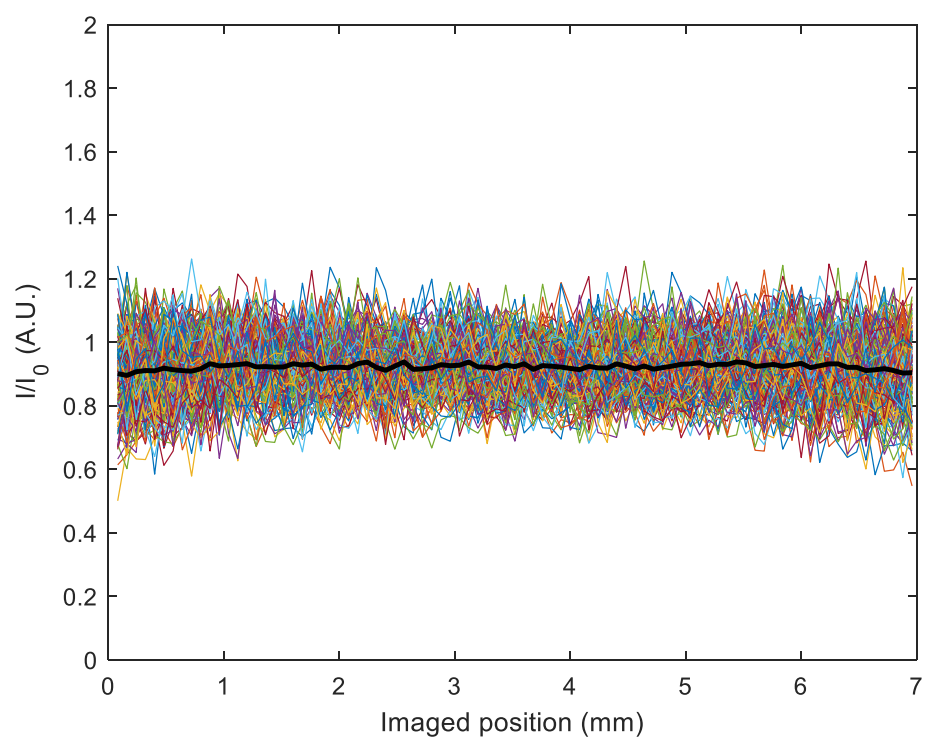


Figure 12: Raw 1-D Rayleigh signal as a function of pixels for pulse 100 in the CH<sub>4</sub>/O<sub>2</sub>/Ar case. No spatial peaks are observed suggesting a local rise in temperature due to filament formation.

narrow, on the order of 100-200  $\mu m$  [12, 20]. The current spatial resolution is 100  $\mu$ m per pixel, which could be smearing this effect. Secondly, if this is the case, it is also possible the laser is never directly interacting with the filament, as our step size was too large. Given the number of shots taken was of the same order as those for the E-FISH measurements, if that signal is real then it is unlikely it would be missed here. A possible explanation, then, is that the actual temperature fluctuation is the same or smaller order than our error bars, which would result in a local variation in temperature of less than approximately  $\pm 20$  K. If this is true, this would suggest that the oxidation chemistry is playing a larger role for the formation of these filaments than the thermal instability, as this deviation is much smaller than the 10-20% listed in the literature [39, 40]. Again, subsequent experiments are required to fully explain this measurement, but it seems plausible that the local heating effect is small, as the measurements do still actually capture the averaged rise quite well, which would result in a large role being played by the oxidation chemistry and formation of preferential ionization channels due to intermediates and product species.

## 4. Conclusion

The effects of plasma assisted low temperature fuel oxidation and pyrolysis on the formation of plasma instability and electric field distribution is explored for a nanosecond repetitively pulsed plasma discharge and spatial and time-resolved diagnostics. The results show clearly that an oxygen/methane stoichiometric mixture to with an argon bath gas resulted in significant filamentation formation in the plasma during a burst of nanosecond pulses. On the other hand, discharges of oxygen/argon and methane argon result in a uniform discharge without any evidence of streamer formation. This result clearly demonstrated that plasma assisted low temperature oxidation of methane promoted the formation of plasma thermal-chemical instability. These filaments travel with the bath gas but at a reduced velocity, suggesting that the formation is tied to changes in ionization potential of species formed during the oxidation process. With a tenfold increase in pulses, the filaments begin to smooth out and re-join into a uniform discharge, demonstrating a thermal component to this instability formation. Averaged electric field measurements show changes in the secondary pulses and secondary discharge formation, but little change in the primary breakdown event. Single shot raw data counts suggest there may be greatly increased localized electric fields present in these filaments on the order of ~100microns. Rayleigh scattering is utilized to study the bulk number density, and accurately captures the averaged temperature rise during the discharge. This data also shows no evidence, however, of increased temperature in the filaments, suggesting either extremely small filamentary structures or the importance of local chemistry in the instability formation.

## Acknowledgments

The authors would like to thank ExxonMobil for providing funding for this research area through its membership in the Princeton E-filliates Partnership of the Andlinger Center for Energy and the Environment. ACR and YJ are grateful to the U.S. Department of Defense for their funding through the National Defense Science & Engineering Graduate (NDSEG) Fellowship program, Princeton SEAS innovation fund and the Andlinger Center for Energy and the Environment (ACEE) grant, DOE-NETL UCFER grant, the DOE Plasma Science Center grant DE-SC0020233, and NSF grant CBET 1903362. TYC was partially supported through the Program in Plasma Science and Technology at Princeton University Fellowship.

### References

- [1] P. Mehta, P. Barboun, F. A. Herrera, J. Kim, P. Rumbach, *et al.*, "Overcoming ammonia synthesis scaling relations with plasma-enabled catalysis," *Nat. Catal.*, vol. 1, no. 4, pp. 269–275, Apr. 2018.
- [2] H. Vach and Q. Brulin, "Controlled Growth of Silicon Nanocrystals in a Plasma Reactor," *Phys. Rev. Lett.*, vol. 95, no. 16, p. 165502, Oct. 2005.
- [3] X. Yang, F. Zhao, Y.-W. Yeh, R. S. Selinsky, Z. Chen, *et al.*, "Nitrogen-plasma treated hafnium oxyhydroxide as an efficient acid-stable electrocatalyst for hydrogen evolution and oxidation reactions," *Nat. Commun.*, vol. 10, no. 1, p. 1543, Apr. 2019.
- [4] X. Zhao, Y. Liu, S. Inoue, T. Suzuki, R. O. Jones, et al., "Smallest Carbon Nanotube Is \$3\text \text \mathrm\AA\$ in Diameter," Phys Rev Lett, vol. 92, no. 12, p. 125502, Mar. 2004.
- [5] D. Z. Pai, D. A. Lacoste, and C. O. Laux, "Transitions between corona, glow, and spark regimes of nanosecond repetitively pulsed discharges in air at atmospheric pressure," *J. Appl. Phys.*, vol. 107, no. 9, p. 093303, 2010.
- [6] M. Simeni Simeni, Y. Tang, Y.-C. Hung, Z. Eckert, K. Frederickson, et al., "Electric field in Ns pulse and AC electric discharges in a hydrogen diffusion flame," Combust. Flame, vol. 197, pp. 254–264, Nov. 2018.
- [7] Y. Tang, M. J. S. Simeni, Q. Yao, K. Frederickson, and I. V. Adamovich, "Flame Oscillations Excited by a Ns Pulse / Ms Tail Electric Discharge Waveform," in *AIAA Scitech 2019 Forum*, American Institute of Aeronautics and Astronautics.
- [8] M. C. Griskey and R. L. Stenzel, "Secondary-Electron-Emission Instability in a Plasma," *Phys. Rev. Lett.*, vol. 82, no. 3, pp. 556–559, Jan. 1999.
- [9] H. Lashinsky, "Universal Instability in a Fully Ionized Inhomogeneous Plasma," *Phys. Rev. Lett.*, vol. 12, no. 5, pp. 121–123, Feb. 1964.
- [10] Y. P. Raizer, Gas Discharge Physics. Berlin: Springer-Verlag, 1991.
- [11] Y. B. Golubovskii, V. Nekuchaev, S. Gorchakov, and D. Uhrlandt, "Contraction of the positive column of discharges in noble gases," *Plasma Sources Sci. Technol.*, vol. 20, no. 5, p. 053002, Sep. 2011.
- [12] M. N. Shneider, M. S. Mokrov, and G. M. Milikh, "Dynamic contraction of the positive column of a self-sustained glow discharge in air flow," *Phys. Plasmas*, vol. 21, no. 3, p. 032122, Mar. 2014.
- [13] M. N. Shneider, M. S. Mokrov, and G. M. Milikh, "Dynamic contraction of the positive column of a self-sustained glow discharge in molecular gas," *Phys. Plasmas*, vol. 19, no. 3, p. 033512, Mar. 2012.
- [14] Y. Ju and W. Sun, "Plasma assisted combustion: Dynamics and chemistry," *Prog. Energy Combust. Sci.*, vol. 48, pp. 21–83, 2015.
- [15] Y. Ju, C. B. Reuter, O. R. Yehia, T. I. Farouk, and S. H. Won, "Dynamics of cool flames," *Prog. Energy Combust. Sci.*, vol. 75, p. 100787, Nov. 2019.
- [16] I. V. Adamovich, M. Nishihara, I. Choi, M. Uddi, and W. R. Lempert, "Energy coupling to the plasma in repetitive nanosecond pulse discharges," *Phys. Plasmas*, vol. 16, no. 11, p. 113505, 2009.
- [17] Z. Yin, "Fuel Oxidation and Ignition by Nanosecond Pulse Discharges at Elevated Temperatures," The Ohio State University, 2013.
- [18] I. Choi, M. Uddi, N. Jiang, I. Adamovich, and W. Lempert, "Stability and Heating Rate of Air and Ethylene-Air Plasmas Sustained by Repetitive Nanosecond Pulses," in 47th AIAA Aerospace Sciences Meeting including The New Horizons Forum and Aerospace Exposition, 0 vols., American Institute of Aeronautics and Astronautics, 2009.
- [19] S. Lanier, S. Bowman, D. Burnette, I. V. Adamovich, and W. R. Lempert, "Time-resolved temperature and O atom measurements in nanosecond pulse discharges in combustible mixtures," *J. Phys. Appl. Phys.*, vol. 47, no. 44, p. 445204, Oct. 2014.
- [20] H. Zhong, M. N. Shneider, M. S. Mokrov, and Y. Ju, "Thermal-chemical instability of weakly ionized plasma in a reactive flow," *J. Phys. Appl. Phys.*, vol. 52, no. 48, p. 484001, Sep. 2019.
- [21] B. M. Goldberg, T. L. Chng, A. Dogariu, and R. B. Miles, "Electric field measurements in a near atmospheric pressure nanosecond pulse discharge with picosecond electric field induced second harmonic generation," *Appl. Phys. Lett.*, vol. 112, no. 6, p. 064102, Feb. 2018.
- [22] A. Dogariu, B. M. Goldberg, S. O'Byrne, and R. B. Miles, "Species-Independent Femtosecond Localized Electric Field Measurement," *Phys. Rev. Appl.*, vol. 7, no. 2, p. 024024, Feb. 2017.
- [23] R. S. Finn and J. F. Ward, "dc-Induced Optical Second-Harmonic Generation in the Inert Gases," *Phys. Rev. Lett.*, vol. 26, no. 6, pp. 285–289, Feb. 1971.
- [24] P. Sitz and R. Yaris, "Frequency Dependence of the Higher Susceptibilities," *J. Chem. Phys.*, vol. 49, no. 8, pp. 3546–3557, Oct. 1968.
- [25] J. E. Retter and G. S. Elliott, "On the possibility of simultaneous temperature, species, and electric field measurements by coupled hybrid fs/ps CARS and EFISHG," *Appl. Opt.*, vol. 58, no. 10, pp. 2557–2566, Apr. 2019.

- [26] Y. Cui, C. Zhuang, and R. Zeng, "Electric field measurements under DC corona discharges in ambient air by electric field induced second harmonic generation," *Appl. Phys. Lett.*, vol. 115, no. 24, p. 244101, Dec. 2019.
- [27] Y. Tang, M. Simeni Simeni, K. Frederickson, Q. Yao, and I. V. Adamovich, "Counterflow diffusion flame oscillations induced by ns pulse electric discharge waveforms," *Combust. Flame*, vol. 206, pp. 239–248, Aug. 2019.
- [28] T. L. Chng, I. S. Orel, S. M. Starikovskaia, and I. V. Adamovich, "Electric field induced second harmonic (E-FISH) generation for characterization of fast ionization wave discharges at moderate and low pressures," *Plasma Sources Sci. Technol.*, vol. 28, no. 4, p. 045004, Apr. 2019.
- [29] B. M. Goldberg, S. Reuter, A. Dogariu, and R. Miles, "1D Spatially Resolved Electric Fields in Atmospheric Pressure Nanosecond Pulse Discharges Using Ultrashort Laser Pulses," in AIAA Scitech 2019 Forum, 0 vols., American Institute of Aeronautics and Astronautics, 2019.
- [30] K. Orr, Y. Tang, M. S. Simeni, D. van den Bekerom, and I. V. Adamovich, "Measurements of electric field in an atmospheric pressure helium plasma jet by the E-FISH method," *Plasma Sources Sci. Technol.*, vol. 29, no. 3, p. 035019, Mar. 2020.
- [31] A. Rousso, X. Mao, Q. Chen, and Y. Ju, "Kinetic studies and mechanism development of plasma assisted pentane combustion," *Proc. Combust. Inst.*, vol. 37, no. 4, pp. 5595–5603, Jan. 2019.
- [32] J. K. Lefkowitz, P. Guo, A. C. Rousso, and Y. Ju, "Species and temperature measurements of methane oxidation in a nanosecond repetitively pulsed discharge," *Phil Trans R Soc A*, vol. 373, no. 2048, 2015.
- [33] T. Y. Chen, A. C. Rousso, S. Wu, B. M. Goldberg, H. van der Meiden, *et al.*, "Time-resolved characterization of plasma properties in a CH4/He nanosecond-pulsed dielectric barrier discharge," *J. Phys. Appl. Phys.*, vol. 52, no. 18, p. 18LT02, Feb. 2019.
- [34] M. S. Simeni, B. Goldberg, I. Gulko, K. Frederickson, and I. V. Adamovich, "Sub-nanosecond resolution electric field measurements during ns pulse breakdown in ambient air," *J. Phys. Appl. Phys.*, vol. 51, no. 1, p. 01LT01, Dec. 2017.
- [35] M. Simeni Simeni, B. M. Goldberg, C. Zhang, K. Frederickson, W. R. Lempert, *et al.*, "Electric field measurements in a nanosecond pulse discharge in atmospheric air," *J. Phys. Appl. Phys.*, vol. 50, no. 18, p. 184002, May 2017.
- [36] A. Rousso, S. Yang, J. Lefkowitz, W. Sun, and Y. Ju, "Low temperature oxidation and pyrolysis of nheptane in nanosecond-pulsed plasma discharges," *Proc. Combust. Inst.*, vol. 36, no. 3, pp. 4105–4112, Jan. 2017.
- [37] J. R. Roth, J. Rahel, X. Dai, and D. M. Sherman, "The physics and phenomenology of One Atmosphere Uniform Glow Discharge Plasma (OAUGDP<sup>TM</sup>) reactors for surface treatment applications," *J. Phys. Appl. Phys.*, vol. 38, no. 4, pp. 555–567, Feb. 2005.
- [38] D. F. Opaits, M. N. Shneider, R. B. Miles, A. V. Likhanskii, and S. O. Macheret, "Surface charge in dielectric barrier discharge plasma actuators," *Phys. Plasmas*, vol. 15, no. 7, p. 073505, Jul. 2008.
- [39] A. Fridman, *Plasma Chemistry*. Cambridge University Press, 2008.
- [40] A. Fridman, A. Chirokov, and A. Gutsol, "Non-thermal atmospheric pressure discharges," *J. Phys. Appl. Phys.*, vol. 38, no. 2, pp. R1–R24, 2005.